Volume 55
Number 13
31 March 2026
Pages 5079-5418

Dalton Transactions

An international journal of inorganic chemistry

rsc.li/dalton

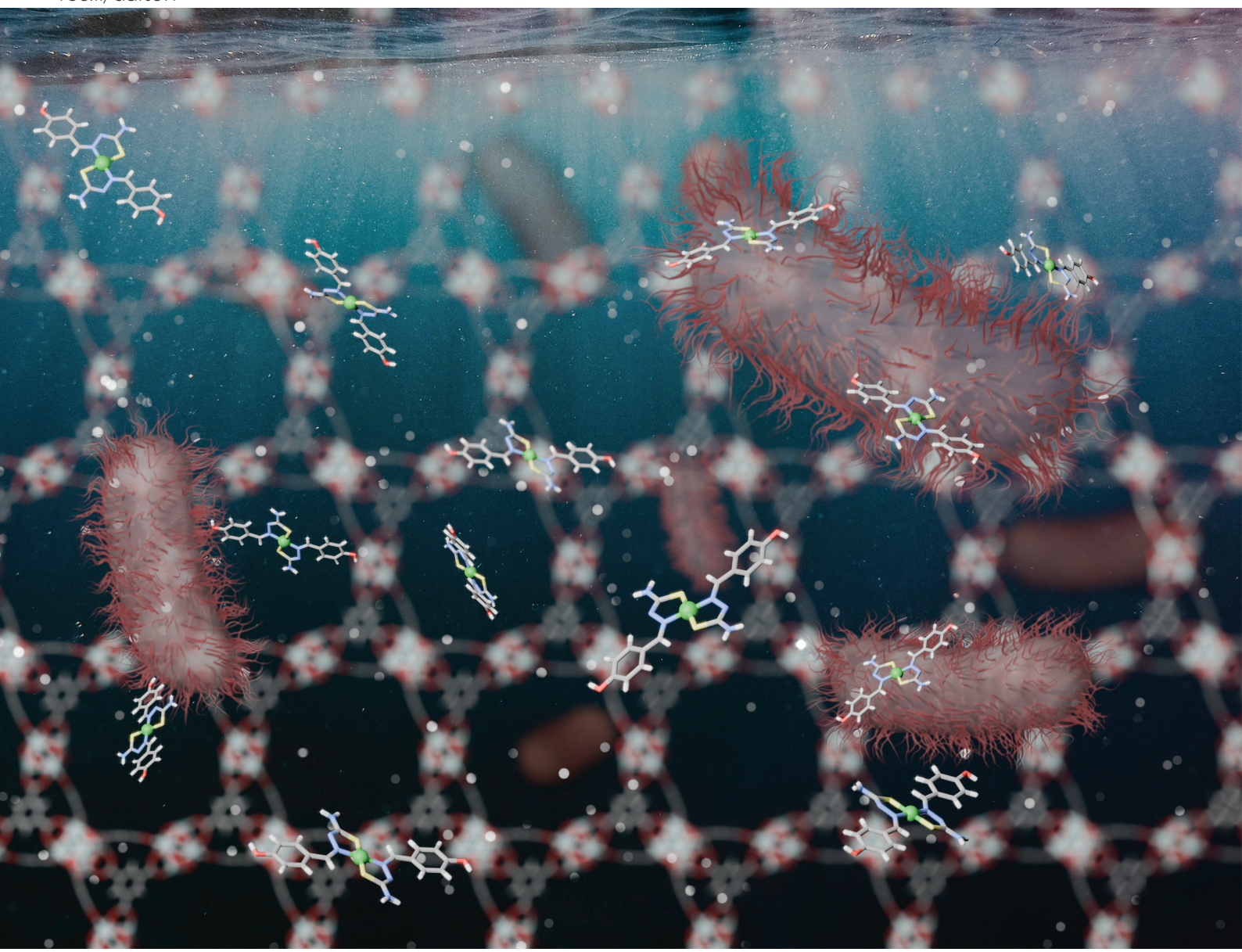

ISSN 1477-9226

ROYAL SOCIETY OF CHEMISTRY

PAPER

Adoracion G. Quiroga *et al.*

Structural features and antibacterial activity of Ni(II) thiosemicarbazones in a zirconium metal-organic framework composite

Dalton Transactions

ROYAL SOCIETY OF CHEMISTRY

PAPER

View Article Online
View Journal | View Issue

Cite this: *Dalton Trans.*, 2026, **55**, 5130

Structural features and antibacterial activity of Ni(II) thiosemicarbazones in a zirconium metal-organic framework composite

Edward Loukopoulos, [a,b] David Fabra, [a] Jorge Melones-Herrero,[c,d,e] Ana I. Matesanz, [a] Carmen Viciana,[a] Ana E. Platero-Prats, *[f] Isabel Sánchez-Pérez *[c,d,e] and Adoracion G. Quiroga *[a,g]

Metal–Organic Frameworks for Biological Applications (BioMOFs) are materials that incorporate therapeutically active ligands into the framework that offer an alternative strategy which combines the structural advantages of MOFs with enhanced functionality for pharmacological properties. The tunable interactions between metal nodes and organic linkers in MOFs favor gradual degradation and/or release of bioactive species. In this work we present the synthesis and detailed characterization of a composite incorporating a Nickel(II) thiosemicarbazone complex and MOF-808. The composite releases Ni(II) species in a controlled manner over 24 h, as demonstrated by UV and NMR. This phenomenon has been applied to inhibit bacterial growth. This research will encourage further exploration into the rational design of new thiosemicarbazones/MOFs materials.

Received 16th December 2025,
Accepted 18th February 2026

DOI: 10.1039/d5dt03008k

rsc.li/dalton

Introduction

Metal–organic frameworks (MOFs) are hybrid materials that have garnered significant interest in biomedical applications due to their high porosity, ability to adsorb and host biologically active compounds. MOFs offer several strategies for drug incorporation: active compounds can be introduced into the internal and/or external surfaces of a preformed MOF structure *via* covalent and/or noncovalent (adsorption) bonding, or they can become constitutive parts of the material structure using therapeutically active cations and/or ligands, forming BioMOFs.[1] Many well-known drugs are hindered by poor water solubility, instability, rapid metabolism, and non-selective biodistribution, leading to lower efficacy under such conditions. The need to effectively manage these issues has therefore driven the development of alternative therapeutic strategies, including design of custom materials as advanced drug delivery systems.

In this context, MOFs have shown particular promise in biological applications[1,2] related to microbial treatment including prevention of bacterial attachment, inhibition of bacterial growth and killing bacteria.[3,4] From a biological standpoint, MOFs can interact with microbial cells at multiple levels *via* several of their inherent features. Through their intrinsic porous architecture, they enable effective encapsulation of antibacterial agents, as well as bacterial metabolites and cell wall components.[5] The vast potential for chemical tuning or functionalizations in MOFs has also led to materials with improved biocompatibility and biodegradability.[6–8] MOF-based materials incorporating bioactive metal centers (such as Zn^{2+}, Cu^{2+}, Ni^{2+}, or Ag^{+}) can disrupt bacterial membranes, generate reactive oxygen species and interfere with essential enzymatic processes, ultimately leading to cell death.[5,9]

While effective, the above strategies can still present limitations in loading capacity or release kinetics.[10] In response, MOF composites that incorporate additional bioactive molecules offer an alternative and promising solution, combining the structural advantages of MOFs with enhanced functionality for antimicrobial properties.[11,12] This strategy can allow us to achieve high loading capacities and sustained release of the encapsulated bioactive species, while incorporating other desirable functions (*e.g.* targeted delivery to specific cells, controlled release depending on pH, temperature, enzymatic activity).[13]

With the above in mind, we set out on developing stable MOF-based composites with potentially enhanced performance in antibacterial applications. For this purpose, we have

[a]*Inorganic Chemistry department. Universidad Autónoma de Madrid (UAM), 28049 Madrid, Spain. E-mail: adoracion.gomez@uam.es*
[b]*Condensed Matter Physics Center (IFIMAC), 28049 Madrid, Spain*
[c]*Department of Biochemistry, Medicine School, UAM, 28049 Madrid, Spain. E-mail: is.perez@uam.es*
[d]*Instituto de Investigaciones Biomédicas "Sols-Morreale" IIBM-CSIC-UAM, 28049 Madrid, Spain*
[e]*BIOPAC-IRYCIS, 28049 Madrid, Spain*
[f]*Institute of Catalysis and Petrochemistry CSIC, 28049 Madrid, Spain. ana.platero-o@icp.csic.es*
[g]*IAdChem-UAM, 28049 Madrid, Spain*

synthesized hybrid materials that combine the well-known zirconium framework MOF-808 with metalloligands based on thiosemicarbazone (TSC) molecules. The main structure of MOF-808 is highly porous (hexagonal pores of 1.8 nm diameter) and water-stable, consisting of unsaturated Zr_6O_8 clusters and benzene-1,3,5-tricarboxylate (BTC) linkers (Fig. 1A). These features provide an ideal platform for incorporation of additional species *via* multiple interactions (*e.g.* coordinative or H-bonding, π···π stacking), easily accommodating further chemical modification or composite design towards targeted functionalities.[14] At the same time, TSCs are Schiff bases with a variety of donor atoms for metal coordination and significant electronic delocalization, enabling binding modes for possible functionalization and sites for metal ions.[15] These compounds have garnered interest within the scientific community due to their wide range of biological properties.[16,17] Their coordination to metal ions (Fig. 1B) enhances their biological activity, often rendering potential metallodrugs more efficacious than the free ligands.[18] The scarcity of examples of sulfur donor ligands contained in MOFs and their pharmacological properties underscores their potential as candidates for the development of novel therapeutic agents.[19]

In this work, we report the synthesis of two new Ni-TSC complexes and their incorporation into the MOF-808 framework to develop functional materials with enhanced antimicrobial activity. Thorough characterization of the resulting composites has been performed to reveal a controlled release of Ni(II) species depending on the initial material composition, which eventually facilitates inhibition of bacterial growth. Our study represents the first attempt to incorporate thiosemicarbazone moieties within a MOF material, and the results highlight the potential promise of these molecules in biological research and antibacterial evaluation.

Results and discussion

Synthesis and characterization of Ni1 and Ni2 complexes

The two Ni(II) complexes used in this work were synthesized in high yields. It was carried out by direct reaction of two equivalents of the respective ligand with one equivalent of $Ni(NO_3)_2{\cdot}6H_2O$ in MeOH and base-catalyzed to shift the tautomeric equilibrium to the thiolate form of the ligand. The reaction also proceeds in water (pH below 8 to prevent NiO formation). In both cases the base ensures quantitative complex formation, yielding **Ni1**, **Ni2** from 87 to 90%. (Scheme 1) The full characterization was performed by elemental analysis, ESI+ mass spectrometry, IR, NMR and single crystal X-ray diffraction techniques (see experimental and SI sections for details).

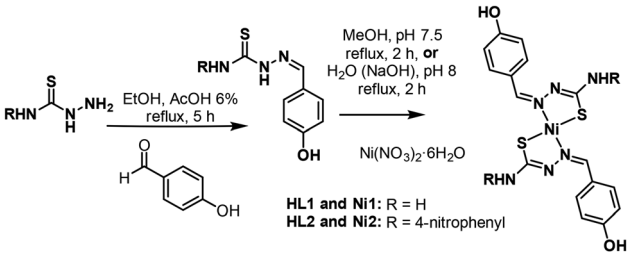

Scheme 1 Synthesis pathway to complexes **Ni1** and **Ni2**.

The analytical data are consistent with 1 : 2 metal : ligand stoichiometry. The ^{1}H-NMR spectra show a single set of signals typical of the AA′BB′ system of *para*-disubstituted aromatic rings, which suggests that the ligands have coordinated in *trans* configuration to the metal. Besides, the signal most affected by the coordination is that of the proton from iminic group which is the closest to the metal ion and has been corroborated by the [^{1}H, ^{13}C] HSQC NMR experiment (Fig. 2 for **Ni1** and Fig. S2 for **Ni2**). The changes in the IR spectra of the complexes suggest that all ligands behave as NS bidentate.

The proposed molecular weight and structure were confirmed by ESI and SC-XRD analysis for the two Ni(II) complexes (Fig. 3). Based on the observed bond angles, the nickel centers adopt a slightly distorted square planar geometry and the Ni–N and Ni–S bond lengths (Table 1) are aligned with those reported for Ni(II)–thiosemicarbazone complexes.[20] The C–S bond distances (~1.73–1.74 Å) fall within the expected range for a single bond, indicating the coordination of the ligand in its deprotonate thiolate form.[21] Additionally, the C–N and N–N bond lengths are intermediate between single and double bonds, suggesting charge delocalization along the TSC skeleton.[22]

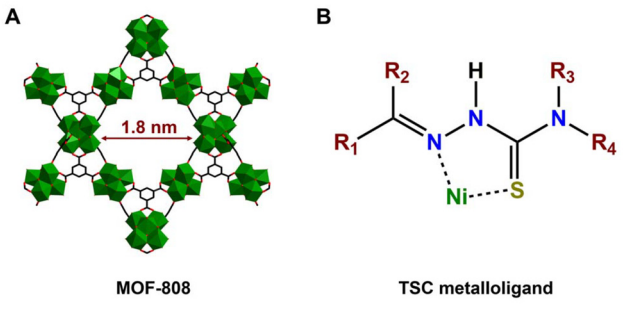

Fig. 1 Structural representation of the MOF-808 (A) and metallo-TSC (B) components used to develop the composite materials of this work. Color code: Zr_6 polyhedra (green), C (black), O (red).

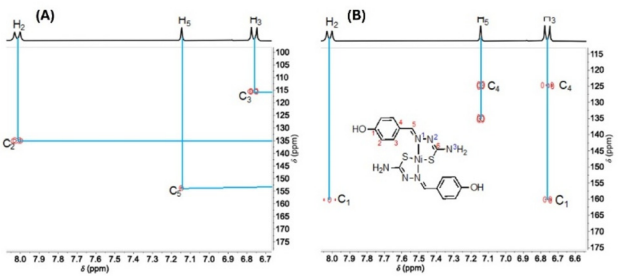

Fig. 2 Aromatic area of the 2D [^{1}H, ^{13}C] NMR. (A) HSQC and (B) HMBC spectra of **Ni1**.

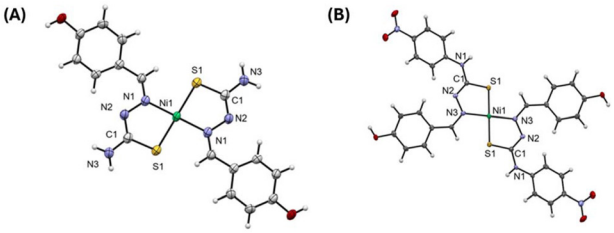

Fig. 3 SC-XRD of the complexes (A) [**Ni1**] and (B) [**Ni2**].

Table 1 Selected bond distances (Å) and angles (°) for complex **Ni1** and **Ni2**

Ni1

Bond lengths (Å)		Bond angles (°)	
C1–N2	1.303(3)	N1#–**Ni1**–N1	180.00(10)
S1–C1	1.737(2)	N3–**Ni1**–S1	84.96(5)
Ni1–S1	2.1666(6)	N1–**Ni1**–S1#	94.16(6)
Ni1–N1	1.9187(19)	N1#–**Ni1**–S1	94.16(6)
N1–N2	1.401(3)	N1#–**Ni1**–S1#	85.84(7)
Ni1–S1#	2.1666(6)	S1–**Ni1**–S1#	180.00

#Symmetry operations: $-x, -y+1, -z+1$

Ni2

Bond lengths (Å)		Bond angles (°)	
C1–N2	1.303(3)	N3#–**Ni1**–N3	180.00(13)
S1–C1	1.737(2)	N3–**Ni1**–S1	84.93(5)
Ni1–S1	2.1666(6)	N3–**Ni1**–S1#	95.04(5)
Ni1–N3	1.9128(17)	N3#–**Ni1**–S1	95.04(5)
N2–N3	1.406(6)	N3#–**Ni1**–S1#	84.96(5)
Ni1–S1#	2.1666(6)	S1–**Ni1**–S1#	180.00

#Symmetry operations: $-x, -y+2, -z+1$

Interestingly, the substituents on the thiosemicarbazone skeleton as well as the presence of crystallization solvent molecules have a great effect on their supramolecular association. In the case of **Ni1**, with an interplane separation between planar molecules of approximately 4.7 Å, the strongest intermolecular forces arise from hydrogen bonds involving amino and hydroxy groups. However, in **Ni2** the distance between adjacent *p*-nitrophenyl aromatic rings of 3.360 Å is optimal for π–π interactions and the hydroxyl groups establish intermolecular hydrogen bonds with dimethylformamide solvent molecules (Fig. S3).

Stability studies of Ni1 and Ni2 in aqueous solutions

The stability assays were conducted in a 1% (v/v) DMSO/Tris 5 mM aqueous solution by monitoring their UV-Vis spectra over 24 h at 37 °C. At a concentration of 20 μM (Fig. 4), the absorbance of **Ni1** remains unchanged while that of **Ni2** rapidly decreases over time, after 5 h only half of the fresh sample absorbance is left. **Ni2** complex was then deemed unsuitable for further functionalization due to this absorbance trend and its susceptibility to hydrolysis in aqueous solutions.

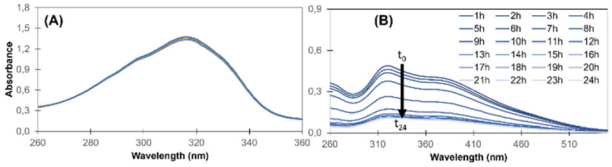

Fig. 4 UV-Vis spectra of **Ni1**(A) and **Ni2**(B) over time. 1% DMSO/Tris 5 mM buffer, 37 °C, $C_{compound}$ = 20 μM.

Assembly of Ni1 within MOF-808

Characterization and stability studies. **Ni1**@MOF-808 composites were successfully prepared *via* mechanochemical synthesis, yielding two materials with 5 : 1 and 1 : 1 stoichiometries. After a washing process, the composites were characterized using FT-IR, ICP-MS, ^{1}H-NMR, N_2 isotherms and PXRD techniques. P-XRD diffractograms (Fig. 5A) show the presence of peaks corresponding to both MOF-808 and **Ni1** phases, confirming that the symmetry and porosity of the MOF framework are retained while the **Ni1** complex remains intact within the composite. The infrared spectrum (Fig. 5B and Fig. S4) of as-made MOF-808 shows main signals related to the organic linker at approximately 1615 (C=C stretching), 1560 (asymmetric COO– stretching), 1440 and 1375 cm^{-1} (COO– symmetric stretching), in full agreement with previous studies.[23] A strong broad peak appears at ~655 cm^{-1}, characteristic of collective vibrations from Zr–O bonds. The corresponding spectra for both Ni@MOF-808 materials retain all these signals, further verifying that the structural integrity of the framework does not alter after composite formation. Additional peaks associated to the **Ni1** complex are observed. Bands corresponding to the *ν*(OH) and *ν*(NH) stretching modes are weaker and less-well resolved compared to **Ni1** and **HL1**, suggesting interactions at the interface that stabilize the incorporation of **Ni1** within the MOF structure. It is important to note that these bands are not strongly affected by the binding of **HL1** to nickel, which involves the deprotonation of NH group. Furthermore, in both **Ni1**@MOF-808 materials the contribution in intensity and signal overlap deriving from each component (MOF-808 and **Ni1**) is fully consistent with the initial synthetic ratio. N_2 adsorption isotherms for these materials (Fig. S5 and Table S1) revealed large decreases in uptake, pore volume and surface area compared to the pristine MOF. As expected, the lowest values for these parameters were observed in the 5 : 1 analogue. Importantly, both **Ni1**@MOF materials

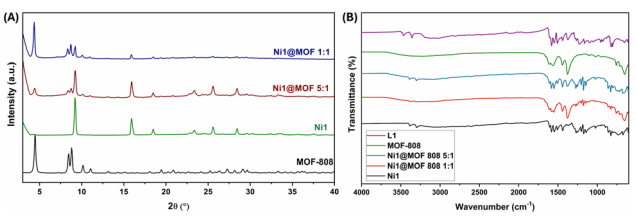

Fig. 5 (A): P-XRD diffractograms and (B) infrared spectra of MOF-808, **Ni1**, **Ni1**@MOF 5 : 1 and **Ni1**@MOF 1 : 1.

exhibited distinct pore size distribution results, with differing contribution of micropores in each case (Fig. S6). These results are in agreement with the presence of composites rather than physical mixtures of two separate components.[24] Overall, the above data confirm successful composite formation in good reproducibility.

To fully evaluate the presence of the Ni-TSCN fragment within the MOF structure, a sample of the composite digested in HF and the proportions of the residual components were analyzed: [L]:(BTC, COO^-), indicating 1.05 and 4.41 respectively (see Table 2). In addition, quantitative assays of the same solid were performed by elemental analysis and ICP-MS which corroborated the ratio expected in the samples *via* stoichiometry, indicating that no complex leaches after washing.

The stability of **Ni1**@MOF-808 (5 : 1) and **Ni1**@MOF-808 (1 : 1) composites in aqueous media was first evaluated through comparison of their PXRD patterns before and after exposure to pure water and aqueous buffered solutions (Tris 5 mM, RPMI medium and phosphate buffer 20 mM) as shown in Fig. 6 and Fig. S7.

The characteristic diffraction peaks of the two phases (MOF-808 and **Ni1**) are preserved for both materials in all tests. A notable decrease in intensity is observed for the main signals contributed by MOF-808 in the low angle region, in agreement with pore filling by solvent molecules. Upon treatment with phosphate buffer, the materials exhibit increased diffuse scattering at 2θ = ~25°, indicating reduced long-range order in comparison to the as-made analogues. The absence of a similar feature in the other aqueous buffers indicates that this effect is unlikely to arise solely from solvent-induced disorder and instead points to a degree of structural amorphization under phosphate treatment conditions. The slight decrease in the intensity of some peaks associated with **Ni1** suggests minor complex leaching, and this behavior is consistent with the colloidal stability results obtained from the DLS studies. As it is shown in Table 3, MOF-808 as well as **Ni1**@MOF-808 5 : 1 and 1 : 1 maintain a constant particle size over the first 24 hours.[25] To further investigate the stability of the new **Ni1**@MOF-808 composite materials, a series of pH-dependent experiments were conducted. D_2O suspensions of **Ni1**@MOF samples were monitored over time using ^{1}H-NMR, measuring the initial and final pHs. At time zero, a set of signals corresponding to a Ni(II)–thiosemicarbazone species was observed for both **Ni1**@MOF-808 composites, obtaining for 5 : 1 (Fig. 7) the spectra with better resolution than 1 : 1 (data not shown). These signals did not correspond to the orig-

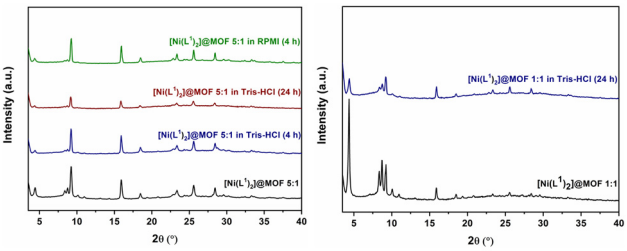

Fig. 6 Stability determined by PXRD of **Ni1**@MOF 5 : 1 and **Ni1**@MOF 1 : 1 in different media.

Table 3 Particle size and ζ-potential (surface charge) for MOF-808, of **Ni1**@MOF 5 : 1 and **Ni1**@MOF 1 : 1 in water after suspension and 24 h incubation time

	MOF-808	
Time (h)	0	24
Size (nm)	690 ± 7	685 ± 3
ζ-potential (mV)	+35 ± 2	+31 ± 1
	Ni1@MOF 5 : 1	
Time (h)	0	0
Size (nm)	1490 ± 50	1490 ± 50
ζ-potential (mV)	−49 ± 1	−49 ± 1
	Ni1@MOF 1 : 1	
Time (h)	0	0
Size (nm)	1115 ± 62	1115 ± 62
ζ-potential (mV)	−37 ± 6	−37 ± 6

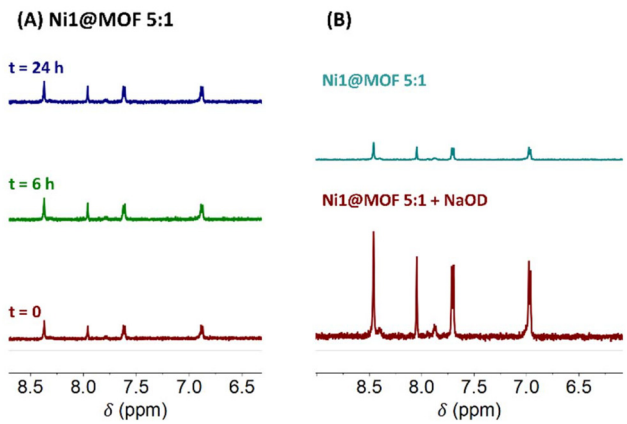

Fig. 7 ^{1}H-NMR stability of (A) **Ni1**@MOF 5 : 1 over the time. (B) ^{1}H-NMR of **Ni1**@MOF 5 : 1 in D_2O (pH 5.6) and after addition of NaOD (pH 10.1).

Table 2 Elemental analysis, ICP-MS, ^{1}H-NMR results. ^{1}H-NMR sample digested in HF

	Elemental analysis						
Sample	%C	%H	%N	%S	Ratio	^{1}H-NMR	ICP-MS
Ni1@MOF 1 : 1	32.98 $Zr_6O_4(OH)_{10}(C_9H_3O_6)_2(H_2O)_5(C_{16}H_{16}N_6NiO_2S_2)_1$	3.40	11.22	8.32	1.04	1.05	1.03
Ni1@MOF 5 : 1	23.42 $Zr_6O_4(OH)_{10}(C_9H_3O_6)_2(H_2O)_1(C_{16}H_{16}N_6NiO_2S_2)_5$	3.18	4.76	3.31	4.62	4.41	4.55

inal **Ni1** complex and did not increase in intensity over time (Fig. 7(A)). Upon addition of 0.1 M NaOD in D_2O, the intensity of these signals increased, and the solution turned light green, indicating the release of water-soluble Ni(II) species (Fig. 7(B)).

In parallel, a titration of the **Ni1**@MOF 5 : 1 was carried out using an automatic burette (Titrando®) to evaluate Ni(II) leaching from suspensions of the composites in water. The pH of the suspension was first decreased to 2 using HCl 0.1 M and then titrated with 0.1 M NaOH to pH 12.5. The solution remained colorless down to pH 2. A color change from colorless to light green was observed at pH 6.54, suggesting the start of Ni(II) species release. At pH values above 8.9, the solution turned dark brown, indicative of partial oxidation or degradation of the MOF structure. As shown in Fig. 8 the equivalence point of the titration occurred at pH 6.54, correlating with the appearance of Ni(II) species, in the ^{1}H-NMR results (Fig. 7(B)).

Study of the lixiviation with biological buffers

Once the pH was identified as a key factor influencing the leaching of Ni(II) species from **Ni1**@MOF composites, a similar study was conducted in Milli-Q water and various biological buffers using UV-Vis spectroscopy. The initial pH values of the media were 6.8 for Milli-Q water, 7.4 for Tris buffer (5 mM), and 6.2 for phosphate buffer (20 mM). The solutions were initially colorless and upon dispersion of the **Ni1**@MOF composites, a faint green color developed in each case, being stronger and easier to follow in the **Ni1**@MOF 5 : 1 composite. By the end of the experiment, the samples exhibited similar coloration. Fig. 9 shows the UV-Vis spectra of both **Ni1**@MOF 5 : 1 samples, where we can observe an increase in absorbance at 317 nm attributed to the release of a new Ni(II) species. Consistently, **Ni1**@MOF 5 : 1 showed greater leaching than **Ni1**@MOF 1 : 1 (Fig. S7) across all media, because of its higher **Ni1** loading. In phosphate buffer (20 mM), the release of Ni(II) species seems to be lower for both composites compared to Tris buffer (5 mM) in which the absorbance at 317 nm reached the saturation limit of the detector, confirming substantial leaching for **Ni1**@MOF 5 : 1.

These results confirm the lixiviation of new Ni(II) species that can be modulated by the concentration of the composite, the pH, and the nature of the medium. More importantly the leached compound differed from the original **Ni1** complex, which is not soluble in water and requires DMSO for detection. The newly released species was found to be soluble in water, indicating the formation of a distinct Ni(II)-based species.

To further investigate the nature of the released species, the lixiviation assay performed in water was scaled up and dried (see experimental part). From this point onward, the experiments were conducted exclusively with the 5 : 1 composite, as the residue from 1 : 1 sample was insufficient for either analysis or biological testing. The lixiviation result from 5 : 1 was analysed by NMR in DMSO (Fig. 10), and in spite of the low resolution, the spectra is showing signals of **HL1** and another set of signals that does not fully correspond to **Ni1** with new doublets arising nearby.

We attempted to force the dissolution of **Ni1** for reaching a control solution to compare with the released species. However, 1 mg of **Ni1** did not dissolve in 150 mL of water. After evaporating the remaining solution to dryness, the small resulting residue was insoluble and could not be characterized spectroscopically. Consequently, we concluded that the nature of our lixiviation species was different.

Antibacterial evaluation

The antibacterial activity of **Ni1**@MOF 5 : 1 was then evaluated in 96-well plates of a DH5α bacterial suspension with an initial absorbance of 0.1. The compounds were added to LB medium, and cisplatin was included as a positive control due to its known antiproliferative effects.[26] As shown in Fig. 11(A), **Ni1**@MOF 5 : 1 delayed bacterial growth within the first 5 hours, exhibiting almost the same antibacterial activity as cisplatin at 100 μM. This effect was dose-dependent, being non-significant at lower concentrations of 25 and 50 μM (Fig. S8).

Furthermore, a significant reduction in proliferation was detected at 7 hours and sustained through 24 hours with cisplatin, and both **Ni1**@MOF composites (Fig. 11(B)). No differences were observed after **Ni1** and MOF-808 treatments confirming that the antibacterial activity is caused by the released

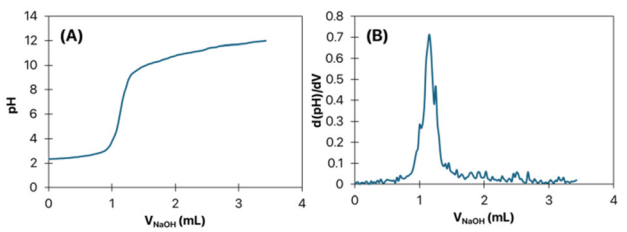

Fig. 8 pH Titration (A) of **Ni1**@MOF (5 : 1) with NaOH and the d(pH)/d*V* *vs.* volume (B).

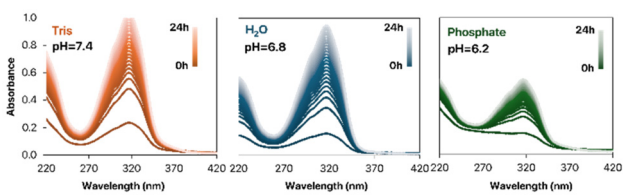

Fig. 9 UV-Visible spectra of **Ni1**@MOF 5 : 1 in Tris-HCl (orange), water (blue) and phosphate buffer (green).

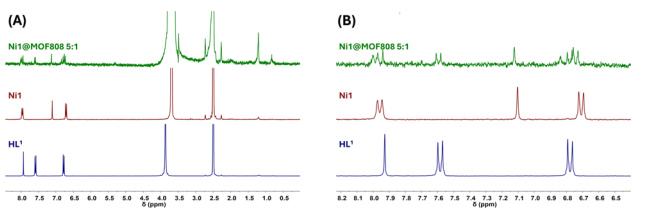

Fig. 10 (A) ^{1}H-NMR from the water supernatant of **Ni1**@MOF 5 : 1 composite compared to **Ni1** complex and **HL1**. (B) Aromatic area detail.

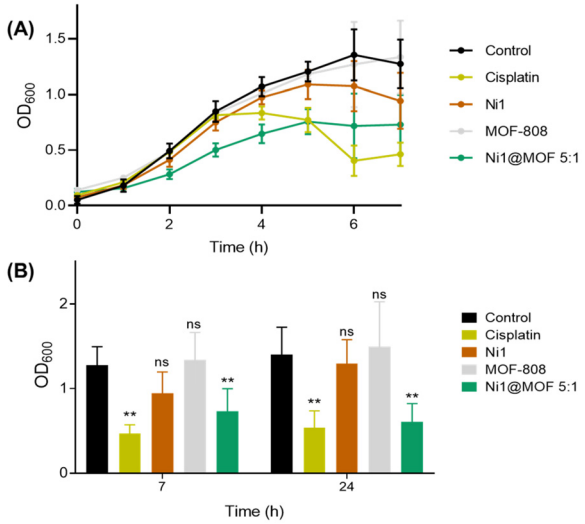

Fig. 11 (A) OD_{600} evolution of DH5α treated with cisplatin, MOF-808, **Ni1**, and **Ni1**@MOF 5 : 1 at 100 μM and (B) the statistical analysis after 7 and 24 h in the presence of the compounds.

product. To the best of our knowledge, this is the first report of a thiosemicarbazone functionalized MOF with antimicrobial activity, paving the way to continue exploring this type of formulation in biological research.

Conclusions

In this work, two new Ni(II) complexes (**Ni1** and **Ni2**) based on thiosemicarbazone ligands have been synthesized and structurally elucidated in detail. **Ni1** has been also successfully integrated within the robust zirconium-based MOF-808 framework to form a new BioMOF composite with controlled release of Ni(II)-based species in water and biological buffers, as determined by thorough studies of its behaviour in solution. Consecutive antimicrobial assays revealed that the composite can effectively inhibit bacterial growth, with its performance arising from the regulated release of these Ni(II)-based species. Overall, this study introduces MOF-thiosemicarbazone composites as potential delivery systems for efficient metal-based antibacterial activity. Our findings show that these materials combine several promising features of biomedical context, including easy syntheses, tuneable loadings, structural stability and controlled delivery of desired species in solution. Future efforts will therefore attempt to further understand and exploit these systems to fully optimize structural behaviour and biological response.

Experimental

Materials and methods

The chemicals and solvents were purchased with "For synthesis" quality from Johnson Matthey, Sigma-Aldrich, and VWR and used without additional purification.

NMR spectra were recorded at room temperature, using a two-channel 300 MHz Bruker Avance III-HD Nanobay spectrometer equipped with a 5 mm BBO 1H/X probe and *Z* gradients. DMSO-d_6 and D_2O were used a solvents (containing 0.05% (v/v) tetramethylsilane (TMS) as a reference). Chemical shift values are given in parts per million (ppm) relative to the residual TMS signals. The following abbreviations were used: s (singlet), bs (broad singlet), d (doublet), and m (multiplet). ICP-MS and elemental analysis were performed on a Nexion 300×, and LECO CHNS-932. Mass spectra were recorded using MALDI (matrix-assisted laser desorption/ionization) with a Bruker Ultraflex III (MALDI-TOF/TOF) mass spectrometry unit and electrospray ionization (ESI) with a Qstar Pulsar I mass spectrometry unit. These instruments are located at the Interdepartmental Investigation Service of UAM (SIdI-UAM). PXRD patterns were collected using a Bruker D8 diffractometer equipped with a Mo source operating at 1600 W. The samples were ground and placed onto a borosilicate sample holder, and the surface was levelled with a clean microscope slide. The diffraction patterns were collected in continuous mode over a 2θ range of 3° to 45°, with a step size of 0.02° and an exposure time of 0.5 s per step. Infrared (IR) spectra were recorded using a PerkinElmer Model 283 spectrometer with an attenuated total reflectance (ATR) MIRacle Single Reflection Horizontal accessory. Low pressure N2 sorption measurements were recorded at 77 K using a Micromeritics 3Flex Surface and Catalyst Characterization Analyzer system. Prior to analysis, the samples were activated under dynamic vacuum at 150 °C for 15 hours to remove all solvent molecules from the pores. UV-visible spectra were recorded using a Thermo Evolution 260 spectrophotometer equipped with temperature control within ±0.1 °C. Particle size and ζ-potential determinations were performed using a Malvern Nano-ZS, Zetasizer Nano series. The pH of the solutions was measured in a Crison Instruments GLP21 pH meter. The adjustment of the pH and the titrations were done with Metrohm instrument, Titrando 905 connected to a Dosino, adjusting the parameters dosing rate, maximum volume, agitation rate and waiting time for the measurements.

Synthesis of the compounds

Ligand synthesis. The ligands are prepared by condensation of the 4-hydroybenzaldehyde and the corresponding thiosemicarbazide, as reported in the literature.[27] Briefly 0.03 mol of thiosemicarbazide is dissolved in 6% aqueous AcOH. This process requires time and 40 °C temperature until complete dissolution. Subsequently, a solution of the aldehyde (0.03 mol) in ethanol is added and kept at reflux for 5 hours. The resulting solid is filtered, washed with 6% aqueous AcOH and ethyl ether and dried under vacuum. Synthesis of **HL2** required *p*-nitrophenylthiosemicarbazide as starting material, which is not commercially available, and was prepared following similar protocol to the already published.[28]

HL1: Off-white solid. Yield: 62%.^{1}H-NMR [DMSO-d_6], δ(ppm): 6.77 (d, 2H, J_{HH} = 8.9 Hz, H_2); 7.60 (d, 2H, J_{HH} = 8.9 Hz, H_3); 7.79 (s, 1H, N^3H_2)*; 7.95 (s, 1H, H_5); 8.02 (s, 1H, N^3H_2)

; 9.83 (s, 1H, N^2H); 11.22 (s, 1H, OH)*. ^{13}C-NMR [DMSO-d_6], δ(ppm): 115.5 (C_2), 125.1 (C_4), 129.0 (C_3), 142.7 (C_5), 159.2 (C_1), 177.4 (C_6). IR (cm^{-1}): $\nu_{as}(NH_2)$: 3470; $\nu_s(NH_2)$: 3358; ν(OH): 3188; ν(C═N): 1579; ν(C═S): 843. ESI-MS (*m*/*z*): 196.05 $[M+H]^+$. Elemental analysis for $C_8H_8N_3OS$ (%): experimental: C: 48.85, H: 4.79, N: 21.41, theoretical: C: 49.21, H: 4.65, N: 21.25. *Interchanges with D_2O.

HL2: Yellow solid. Yield: 69%.^{1}H-NMR [DMSO-d_6], δ(ppm): 6.87 (d, 2H, J_{HH} = 8.8 Hz, H_2); 7.75 (s, 1H, H_5); 7.83 (d, 2H, J_{HH} = 9.3 Hz, H_8); 8.06 (d, 2H, J_{HH} = 9.3 Hz, H_3); 8.19 (d, 2H, J_{HH} = 9.3 Hz, H_9); 10.00 (s,1H, N^2H)*; 10.37 (s,1H, N^3H)*; 12.73 (s,1H, OH)*. ^{13}C-NMR [DMSO-d_6], δ(ppm): 115.6 (C_2), 123.7 (C_9), 124.1 (C_8), 124.6 (C_4), 129.7 (C_3), 143.3 (C_{10}), 144.6 (C_7), 145.5 (C_5), 159.8 (C_1), 174.6 (C_6). ESI-MS (*m*/*z*): $[M+H]^+$: 316. IR (cm^{-1}): $\nu_{as}(NH_2)$: 3391; $\nu_s(NH_2)$: 3358; ν(OH): 3208; $\nu_{as}(NO_2)$: 1479; ν(C═N): 1524; $\nu_s(NO_2)$: 1300; ν(C═S): 854. Elemental analysis for $C_{14}H_{12}N_4O_3S{\cdot}0.9H_2O$ (%): experimental: C: 50.57, H: 4.42, N: 16.86, calculated: C: 50.29, H: 4.22, N: 16.70. *Interchanges with D_2O. A single crystal was resolved by X-Ray diffraction (not yet reported) and the figure and structural data is collected in Fig. S1 and Table S2.

Ni(II) complexes syntheses

A general method is followed for the syntheses of the complexes. In a round bottom flask, the corresponding ligand (**HL1** or **HL2**) (2 mmol) is dissolved in methanol and a methanolic solution of $Ni(NO_3)_2{\cdot}6H_2O$ (2 mmol) is added dropwise. Subsequently, the solution is brought to pH 7.5 using 0.5 M NaOH and a precipitate is immediately observed. The reaction mixture is kept at reflux for 2 h, the solid is filtered, washed with distilled water, methanol and ethyl ether, and dried under vacuum. The reaction is also carried out using water instead of methanol as a solvent and the complexes and the yield are still maintained.

Ni1: **$[Ni(L^1)_2]$**: Dark green solid. Yield: 87%. ^{1}H-NMR [DMSO-d_6], δ(ppm): 6.75 (d, 2H, J_{HH} = 8.9 Hz, H3); 6.89 (s, 1H, NH2)*; 7.14 (s, 1H, H5); 8.02 (d, 2H, J_{HH} = 8.9 Hz, H2); 10.18 (s, 1H, OH)*. ^{13}C-NMR [DMSO-d6], δ(ppm): 115.2 (C_2), 124.3 (C_4), 134.7(C_3), 153.4 (C_5), 159.8 (C_1). MALDI-MS (*m*/*z*): 447.1 $[M+H]^+$. IR (cm^{-1}): $\nu_{as}(NH_2)$: 3673; $\nu_s(NH_2)$: 3452; ν(OH): 3120; ν(C═N): 1570; ν(C–S): 812–799. Elemental analysis for $C_{16}H_{16}N_6NiO_2S_2{\cdot}0.5H_2O$ (%): experimental: C: 42.41, H: 4.02, N: 18.49, calculated: C: 42.13, H: 3.76, N: 18.42. *Interchanges with D_2O.

Ni2: **$[Ni(L^2)_2]$**: Russet solid. Yield: 88%.^{1}H-NMR [DMSO-d_6], δ(ppm): 6.85 (d, 2H, J_{HH} = 8.1 Hz, H_2), 7.75 (s, 1H, H_5), 7.84 (d, 2H, J_{HH} = 9.4 Hz, H_8), 8.07 (d, 2H, J_{HH} = 8.1 Hz, H_3), 8.20 (d, 2H, J_{HH} = 9.4 Hz, H_9), 10.36 (s, 1H, OH)*. ^{13}C-NMR [DMSO-d_6], δ(ppm): 115.0 (C_2), 124.7 (C_9), 117.9 (C_8), 123.6(C_4), 134.1 (C_3), 141.1(C_{10}), 146.7 (C_7), 158.1(C_5), 161.1 (C_1). ESI-MS (*m*/*z*): 689.05 $[M+H]^+$. IR (cm^{-1}): $\nu_{as}(NH_2)$: 3392; $\nu_s(NH_2)$: 3357; ν(OH): 3208; $\nu_{as}(NO_2)$: 1482; ν(C═N): 1562; $\nu_s(NO_2)$: 1297; ν(C–S): 843–800. Elemental analysis for $C_{28}H_{22}N_8NiO_6S_2{\cdot}2H_2O$ (%): experimental: C: 45.97, H: 3.45, N: 15.75, calculated: C: 46.13, H: 3.65, N: 15.37. *Interchanges with D_2O.

Synthesis of MOF-808 and Ni1@MOF-808 composites

Pristine MOF-808 was synthesized and activated using previously established protocols.[23] The functionalized MOF-808 were obtained through a mechanochemical synthetic approach: the activated MOF-808 (1 equivalent) and the Ni(II) complex [5 equivalents for **Ni1**@MOF-808 (5 : 1), 1 equivalent for **Ni1**@MOF-808 (1 : 1)] were added into a mortar. Using a pestle, the mixture was ground for 30 min in the absence of any solvent to form a homogeneous solid material. The solids were washed with water twice and dried at 60 °C overnight.

Ni1@MOF-808 (1 : 1). Light green powder. Elemental analysis for $Zr_6O_4(OH)_6(C_9H_3O_6)_2(H_2O)_5(C_{16}H_{16}N_6NiO_2S_2)_1$: experimental: C: 32.98, H: 3.4, N: 11.22, S: 8.32 calculated: C: 32.93, H: 3.36, N: 11.56, S: 8.43. **^{1}H-NMR (HF, D_2O and DMSO-d_6)** (procedure described in section 5.6.1): 8.63 (s, 6H, 2× BTCs); 8.11 (s, 2.57H, 2.55 × $HCOO^-$); 7.58 (d, 4.28H, 1.05 × $[Ni(L^1)_2]$); 6.78 (d, 4.60 H, 1.15 × $[Ni(L^1)_2]$). **ICP-MS**: [Zr] (ppm) = 81.32 and [Ni] (ppm) = 9.01; Ni per Zr_6 cluster = 1.03. **Selected IR peaks (cm^{-1})**: 3388 (w), 3303 (w), 1612 (m), 1584 (m), 1551 (m), 1507 (w), 1443 (m), 1380 (s), 1274 (w), 1252 (w), 1204 (w), 1175 (w), 1144 (w), 829 (m), 759 (w), 654 (s).

Ni1@MOF-808 (5 : 1). Dark green powder. **Elemental analysis** for $Zr_6O_4(OH)_6(C_9H_3O_6)_2(H_2O)_1(C_{16}H_{16}N_6NiO_2S_2)_5$ (%): experimental: C: 23.42, H: 3.18, N: 4.76, S: 3.31 calculated: C: 23.38, H: 3.21, N: 4.20, S: 3.07. **^{1}H-NMR (HF, D_2O and DMSO-d_6)**: 8.63 (s, 6H, 2× BTCs); 8.11 (s, 0.9H, 0.7 × $HCOO^-$); 7.58 (d, 15.61H, 4.2 × $[Ni(L^1)_2]$); 6.78 (d, 18.69H, 4.2 × $[Ni(L^1)_2]$). ICP-MS: [Zr] (ppm) = 36.82 and [Ni] (ppm) = 18.31; Ni per Zr_6 cluster = 4.6. **Selected IR peaks (cm^{-1})**: 3388 (w), 3303 (w), 1610 (w), 1585 (m), 1550 (m), 1509 (w), 1442 (m), 1380 (m), 1273 (m), 1250 (m), 1204 (w), 1175 (m), 1144 (w), 829 (m), 764 (w), 676 (w).

The samples to collect PXRD patterns were ground and placed onto a borosilicate sample holder, and the surface was levelled with a clean microscope slide. The diffraction patterns were collected in continuous mode over a 2θ range of 3° to 45°, with a step size of 0.02° and an exposure time of 0.5 s per step.

Sample preparation and aqueous buffer stability *via* PXRD

Initially, 5 mg of the targeted composite material was immersed in 3 ml of the corresponding aqueous buffer solution for a predetermined amount of time (4–24 h). The solid was isolated *via* centrifugation, washed copiously with water and acetone, then dried at 60 °C for 1 hour before PXRD data collection. All stability tests were conducted on separate portions from the same initial batch of material.

Sample preparation and stability measured by DLS

The particle size and ζ-potential of MOF-808, **Ni1**@MOF-808 1 : 1 and **Ni1**@MOF-808 5 : 1 were monitored over a 24 h period following the procedure already published.[18] For these measurements, 1 mg of the respective MOF was suspended in 5 mL of Milli-Q water. The equipment used is a Malvern Zetasizer Nano ZS, sited in IMDEA Nanociencia. The cuvettes

used for the measurements of Potential-ζ were Malvern Zetasizer Cuvettes Disposable. The samples were kept under constant agitation and at 37 °C in a ThermoMixer C Eppendorf.

Lixiviation experiments by UV-Vis and NMR

The preparation of the stock solutions for the lixiviation studies was made dispersing 0.5 mg of **Ni1@MOF-808** (**5 : 1** or **1 : 1**) in 0.250 mL of water solution, this stock is prepared using a Vortex more than 3 minutes to achieve a homogeneous dispersion for reliable data. The samples are then prepared by dilution of the stock until 20 mM (2 mL) in Milli-Q water, Tris-HCl 5 mM (pH 7.4) or phosphate buffer 20 mM (this solution is prepared following the procedure described in the bibliography).[29] Subsequently, the pH was measured for each sample and then the UV-Vis spectra are monitored from 220 to 700 nm, every hour for 24 hours, maintaining the samples with constant stirring and 37 °C.

A pure sample of the functionalized **Ni1@MOF-808 5 : 1** (1 mg) was dispersed in 0.5 mL of D_2O and the ^{1}H-NMR spectra was recorded at 0, 6 and 24 hours. After monitoring the sample, one drop of NaOD 10 mM was added (pH changed from 8.80 to 10.1) and then the ^{1}H-NMR spectra were recorded again. The suspension from the lixiviation studies in water after 24 h was centrifuged. The liquid was dried to residue in an Eppendorf concentrator plus at 45 degrees in 4 h.

Single-crystal X-ray diffraction (SC-XRD)

Molecular structures were determined in SIdI-UAM, using a Bruker X8 Kappa Apex II CCD diffractometer equipped with an Apex-II CCD area detector and a graphite monochromator. For all compounds, the software package SHELTX was used for space group determination, structure solution, and refinement (SHELTXTL-NTversion 6.12, Structure Determination Package, Bruker-Nonius XS, Madison, Wisconsin USA, 1997–2001). The structures were solved by direct methods, completed with difference Fourier syntheses, and refined with anisotropic displacement parameters. Hydrogen atom positions were calculated geometrically and refined using the riding model. Crystal data are collected in Table 4. The respective CCDC IDs contain SI crystallographic data for the compounds.

Bacterial culture

The DH5α wild type strain (ThermoFischer) was grown on LB medium (Sigma-Aldrich) at 37 °C for 24 h. For the determination of antimicrobial activity in liquid culture, DH5α cells were seeded in 96-well plates with an initial absorbance of 0.1. To measure bacterial growth, absorption at an optical density at 600 nm was detected on a SPECTROstar Nano plate reader (BMG Labtech, located at IIBM-CSIC-UAM). Data acquisition and data analysis were performed by using MARS software and Microsoft Excel 365. Statistical analyses were performed using GraphPad prism 8.0 one-way ANOVA with Dunnett post-test. Values of $^*p < 0.05$ were considered significant.

Table 4 Crystal data and structure refinement results for **Ni2** and **Ni1**

Compound/CCDC	**Ni2**/2476950	**Ni1**/2476949
Chemical formula	$C_{40}H_{50}N_{12}NiO_{10}S_2$	$C_{20}H_{26}N_8NiS_2$
Formula weight (g mol^{-1})	981.75	501.30
Temperature (K)	150(2)	296(2)
Crystal system	Triclinic	Monoclinic
Wavelength (Å)	0.71073	0.71073
Space group	$P\bar{1}$	$P121/n1$
Crystal size (mm)	0.009 × 0.066 × 0.165	0.030 × 0.040 × 0.100
Crystal habit	Bright orange-brown ribbon	Dark brown needle
Cell unit dimensions		
a (Å)	10.4885(5)	7.1806(6)
b (Å)	7.4108(3)	11.4484(9)
c (Å)	15.3744(6)	13.8901(10)
α (°)	90	76.331(2)
β (°)	107.141(2)	86.624(3)
γ (°)	90	83.694(3)
Volume (Å^3)	1102.16(15)	1141.94(8)
Z	1	2
Density, calculated (g cm^{-3})	1.479	1.458
Absorption coefficient (mm^{-1})	0.607	1.057

Author contributions

Conceptualization: E. L., A. I. M., A. E. P. P., I. S. P. and A. G. Q. Methodology: E. L., D. F., J. M. H. Validation: E. L., D. F., J. M. H. Formal Analysis: D. F., J. M. H., C. V. Investigation: E. L., D. F., J. M. H., C. V. Resources: A. E. P. P., I. S. P. and A. G. Q. Writing original draft: D. F., J. M. H. Visualization: A. E. P. P., A. I. M., I. S. P. and A. G. Q. Supervision: A. I. M., A. E. P. P., I. S. P. and A. G. Q. Project administration: I. S. P. and A. G. Q. Writing – review & editing: E. L., A. I. M., A. E. P. P., I. S. P. and A. G. Q. Funding acquisition: A. E. P. P., I. S. P. and A. G. Q.

Conflicts of interest

There are no conflicts to declare.

Data availability

The data supporting this article have been included as part of the supplementary information (SI). Supplementary information: SC-XRD figure and crystal data of the ligand HL_2. CCDC number: 2477479; 2D [^{1}H, ^{13}C] NMR for **Ni2**; FT-IR spectra for pristine MOF-808 and the composite materials of this study; information of N2 isotherm (linear scale) recorded at 77 K; nitrogen uptake, pore volume (calculated at p/p_0 = 0.95) and BET surface area values, all for pristine MOF-808 and the composite materials of this study; stability of **Ni1**@MOF 5 : 1 and **Ni1**@MOF 1 : 1 in phosphate buffer (20 mM), as determined by PXRD and UV-Visible spectra of **Ni1**@MOF 1 : 1 in Tris-HCl, water and phosphate buffer. See DOI: https://doi.org/10.1039/d5dt03008k.

The software package SHELTX was used for space group determination, structure solution, and refinement

(SHELTXTL-NTversion 6.12, Structure Determination Package, Bruker-Nonius XS, Madison, Wisconsin USA, 1997–2001).

CCDC 2476950, 2476949 and 2477479 contain the supplementary crystallographic data for this paper.[30a,b,c]

Acknowledgements

This research was funded by Spanish MCIN/AEI/FEDER (10.13039/501100011033) PID2022-137373OB-I00. APP thanks to CNS2022-135261, RYC2018-024328-I and PID2021-123839OB-I00 funded by MICIU/AEI/10.13039/501100011033 and the NextGeneration EU/PRTRTEC-2024/TEC-308 funded by Regional Government of Madrid. E. L. acknowledges financial support from the European Union's Horizon 2020 research and innovation programme under grant agreement No. 101034324 and the "María de Maeztu" Programme for Units of Excellence in R&D (CEX2023-001316-M). JMH was supported by a grant FPI-UAM 2021 from Universidad Autónoma de Madrid (Molecular BioSciences PhD programme). We thank Javier Montero for his contribution to early testing.

References

1 S. Rojas, T. Devic and P. Horcajada, *J. Mater. Chem. B*, 2017, **5**, 2560–2573.
2 I. Imaz, M. Rubio-Martínez, J. An, I. Solé-Font, N. L. Rosi and D. Maspoch, *Chem. Commun.*, 2011, **47**, 7287–7302.
3 D. Han, X. Liu and S. Wu, *Chem. Soc. Rev.*, 2022, **51**, 7138–7169.
4 S. L. Anderson and K. C. Stylianou, *Coord. Chem. Rev.*, 2017, **349**, 102–128.
5 G. Wyszogrodzka, B. Marszałek, B. Gil and P. Dorożyński, *Drug Discovery Today*, 2016, **21**, 1009–1018.
6 L. Guo, W. Kong, Y. Che, C. Liu, S. Zhang, H. Liu, Y. Tang, X. Yang, J. Zhang and C. Xu, *Int. J. Biol. Macromol.*, 2024, **261**, 129799.
7 A. Arenas-Vivo, G. Amariei, S. Aguado, R. Rosal and P. Horcajada, *Acta Biomater.*, 2019, **97**, 490–500.
8 C. Tamames-Tabar, E. Imbuluzqueta, N. Guillou, C. Serre, S. R. Miller, E. Elkaïm, P. Horcajada and M. J. Blanco-Prieto, *CrystEngComm*, 2015, **17**, 456–462.
9 M. Wang, R. Li, S. Sheng, H. Yang, X. Tang, J. Wang, F. Wang, Q. Zhang, L. Bai, X. Chen, J. Gao, X. Ren, H. Liu and J. Su, *Nano Today*, 2025, **63**, 102753.
10 W. Nong, J. Wu, R. A. Ghiladi and Y. Guan, *Coord. Chem. Rev.*, 2021, **442**, 214007.
11 D. Han, Y. Han, J. Li, X. Liu, K. W. K. Yeung, Y. Zheng, Z. Cui, X. Yang, Y. Liang, Z. Li, S. Zhu, X. Yuan, X. Feng, C. Yang and S. Wu, *Appl. Catal., B*, 2020, **261**, 118248.
12 H.-X. Feng, Z. Zhou, J. Jiang, Y.-F. Hui, B.-X. Li, S. Li, H. Guo, F.-Q. Tang, Z.-J. Lin and L.-P. Yan, *Inorg. Chem.*, 2025, **64**, 3541–3552.
13 M. Moharramnejad, A. Ehsani, M. Shahi, S. Gharanli, H. Saremi, R. E. Malekshah, Z. S. Basmenj, S. Salmani and M. Mohammadi, *J. Drug Delivery Sci. Technol.*, 2023, **81**, 104285.
14 G. Lee, I. Ahmed, M. A. Hossain, H. J. Lee and S. H. Jhung, *Coord. Chem. Rev.*, 2025, **524**, 216325.
15 B. Fischer, K. Kryeziu, S. Kallus, P. Heffeter, W. Berger, C. R. Kowol and B. K. Keppler, *RSC Adv.*, 2016, **6**, 55848–55859.
16 D. Fabra, G. Amariei, D. Ruiz-Camino, A. I. Matesanz, R. Rosal, A. G. Quiroga, P. Horcajada and T. Hidalgo, *Mol. Pharm.*, 2024, **21**, 1987–1997.
17 J. H. Bormio Nunes, S. Hager, M. Mathuber, V. Pósa, A. Roller, É. A. Enyedy, A. Stefanelli, W. Berger, B. K. Keppler, P. Heffeter and C. R. Kowol, *J. Med. Chem.*, 2020, **63**, 13719–13732.
18 T. Hidalgo, D. Fabra, R. Allende, A. I. Matesanz, P. Horcajada, T. Biver and A. G. Quiroga, *Inorg. Chem. Front.*, 2023, **10**, 1986.
19 S. B. Zahra, A. Khan, N. Ahmed, M. Rafique, L. Fatima, I. Khan, J. Hussain, S. Khalid, H. A. Ogaly, M. M. Ahmed, A. Al-Harrasi and Z. Shafiq, *J. Mol. Struct.*, 2025, **1322**, 140511.
20 U. M. Osman, S. Silvarajoo, M. F. Noor Hassim, S. Arshad, A. H. Anizaim and F. I. Abdul Razak, *Bioinorg. Chem. Appl.*, 2021, **2021**, 5536902.
21 A. I. Matesanz, E. Jimenez-Faraco, M. C. Ruiz, L. M. Balsa, C. Navarro-Ranninger, I. E. León and A. G. Quiroga, *Inorg. Chem. Front.*, 2018, **5**, 73–83.
22 F. H. Allen, D. G. Watson, L. Brammer, A. G. Orpen and R. Taylor, in *International Tables for Crystallography*, John Wiley & Sons, Ltd, 2006, pp. 790–811.
23 I. Romero-Muñiz, C. Romero-Muñiz, I. Del Castillo-Velilla, C. Marini, S. Calero, F. Zamora and A. E. Platero-Prats, *ACS Appl. Mater. Interfaces*, 2022, **14**, 27040–27047.
24 I. del Castillo-Velilla, C. Castillo-Blas, T. D. Bennett, B. Cuadrado-Benavent, F. Zamora, C. Montoro and A. E. Platero-Prats, *J. Mater. Chem. A*, 2025, **13**, 40665–40671.
25 I. Abánades Lázaro and R. S. Forgan, *Coord. Chem. Rev.*, 2019, **380**, 230–259.
26 A. Gupta, L. Bernacchia and N. M. Kad, *Lett. Appl. Microbiol.*, 2022, **75**, 951–956.
27 A. I. Matesanz, A. B. Caballero, C. Lorenzo, A. Espargaró, R. Sabaté, A. G. Quiroga and P. Gamez, *Inorg. Chem.*, 2020, **59**, 6978–6987.
28 A. I. Matesanz, C. Hernández, A. Rodríguez and P. Souza, *Dalton Trans.*, 2011, **40**, 5738–5745.
29 S. Savir, Z. J. Wei, J. W. K. Liew, I. Vythilingam, Y. A. L. Lim, H. M. Saad, K. S. Sim and K. W. Tan, *J. Mol. Struct.*, 2020, **1211**, 128090–128100.
30 (*a*) CCDC 2476950: Experimental Crystal Structure Determination, 2026, DOI: 10.5517/ccdc.csd.cc2p4gmy; (*b*) CCDC 2476949: Experimental Crystal Structure Determination, 2026, DOI: 10.5517/ccdc.csd.cc2p4glx; (*c*) CCDC 2477479: Experimental Crystal Structure Determination, 2026, DOI: 10.5517/ccdc.csd.cc2p50pl.